

Christos Davatzikos, PhD
Dengfeng Liu, MS
Dinggang Shen, PhD
Edward H. Herskovits, PhD,
MD

Index terms:

Computers, diagnostic aid
Model, mathematical
Spine
Stereotaxis

Published online before print
10.1148/radiol.2243011266
Radiology 2002; 224:919–926

Abbreviations:

AFDM = adaptive focus deformable
model
3D = three-dimensional

¹ From the Center for Biomedical Image Computing, Department of Radiology and Radiological Science (C.D., D.S., E.H.H.), Department of Computer Science (C.D.), and Department of Biomedical Engineering (D.L.), Johns Hopkins University School of Medicine, 601 N Caroline St, JHOC3220, Baltimore, MD 21287. Received July 24, 2001; revision requested September 12; revision received November 19; accepted January 18, 2002. **Address correspondence** to C.D. (e-mail: hristos@jhu.edu).

© RSNA, 2002

Author contributions:

Guarantor of integrity of entire study, C.D.; study concepts, C.D., E.H.H.; study design, all authors; literature research, E.H.H., D.L., C.D.; clinical and experimental studies, all authors; data acquisition, all authors; data analysis/interpretation, D.L., C.D.; statistical analysis, D.L., C.D.; manuscript preparation, D.L., C.D., E.H.H.; manuscript definition of intellectual content, editing, and revision/review, all authors; manuscript final version approval, C.D.

Spatial Normalization of Spine MR Images for Statistical Correlation of Lesions with Clinical Symptoms¹

An image analysis method was developed for spatial normalization of spine magnetic resonance images. A deformable shape model of the spine is first constructed, and it is subsequently used by an automated algorithm to find a shape transformation that places patient data into a stereotaxic space. Very good agreement with manual segmentations was observed. The main application of this method is in lesion-deficit analysis for determining associations between structural damage and clinical symptoms.

© RSNA, 2002

Although low back pain is extremely common and ultimately affects up to 60%–80% of people at some point in their lifetime, depending on the population at study, its causes remain largely unknown (1). A definitive diagnosis is difficult to achieve (2); however, a comprehensive nomenclature, agreed on by the American Society of Neuroradiology, the American Society of Spine Radiology, and the North American Spine Society, is now in place to help in that regard. The principal problem is that patients with persistent pain may have little or no evidence of nerve root compression or mechanical instability; conversely, gross radiologic abnormalities of the spine may be asymptomatic. Despite its importance, low back pain is inadequately understood, diagnosed, and treated (1), and in part, these inadequacies are caused by the lack of comprehensive taxonomy of disorders associated with low back pain (3). Therefore, it is very difficult to deter-

mine precisely what causes someone's pain or to quantify the degree of anatomic abnormality that is necessary to cause persistent clinical symptoms. Thus, the need for rigorous quantitative models for the analysis of image and clinical data in patients with low back pain provided the motivation for the work presented in this article.

Issues similar to those considered in this article have been encountered in lesion-deficit and functional (activation) studies of the brain; these difficulties prompted the brain-mapping community to adopt the now widely used concept of a stereotaxic space, that is, of a canonical space within which structural and functional image data from large cohorts are mapped and analyzed statistically to determine associations between structural, functional, and clinical variables. The concept of a stereotaxic space was initially introduced in studies by Talairach and Tournoux (4). This concept was subsequently adopted widely by the functional imaging community (5–7), by researchers (8,9) in studies linking imaging findings with clinical data, and by investigators (10–19) in studies aiming at statistically characterizing normal and diseased brain morphology.

A key step in a stereotaxic space analysis is spatial normalization, that is, the process of warping a patient's images to match the anatomy of a template that resides in the stereotaxic space. The template can be that of a single individual or of a population average. The development of highly automated and accurate spatial normalization computer algorithms is still an open research problem in the brain imaging community (18,20–25). However, very little attention has been given to other organs, including the spine. Our purpose is to introduce a new

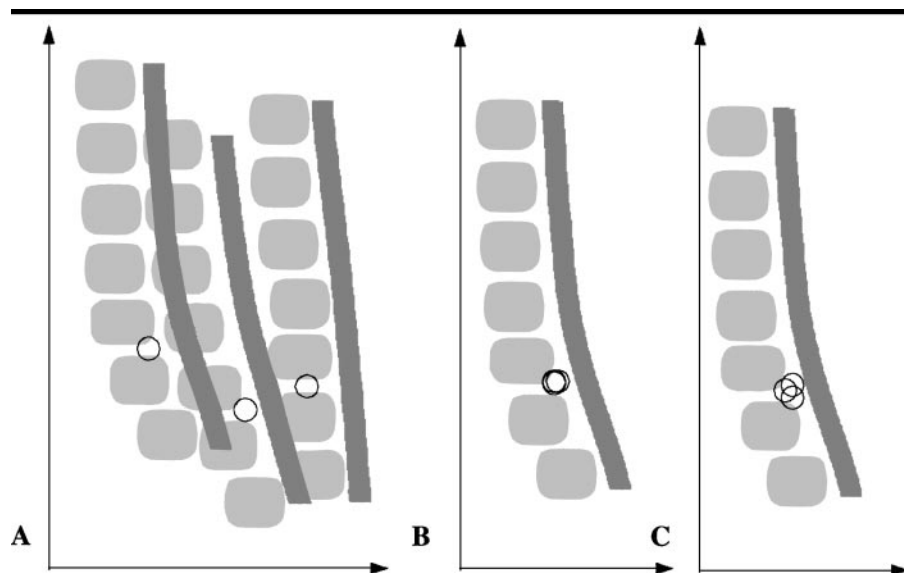


Figure 1. Schematic diagram shows the importance of spatial normalization in placing images from large cohorts into the coordinate system associated with a large image database. *A*, Diagram shows lesions, depicted as small circles, that appear to have different coordinates. Consequently, an image-based statistical query seeking statistical associations between lesion location and clinical symptoms would fail to identify the association, and this failure is caused by loss of statistical power. *B*, Diagram shows that, ideally, interindividual variability in morphology would be entirely eliminated and would, thus, allow lesions in anatomically corresponding locations to have identical coordinates. *C*, Diagram shows that, in practice, if there is enough overlap between the lesions in the stereotaxic space, lesion-pain associations can still be discovered by means of statistical queries.

method for spatial normalization of magnetic resonance (MR) spine images. Additional concepts about spatial normalization are included in the Appendix. A schematic (Fig 1) shows the role of spatial normalization.

Materials and Methods

Background

Our approach to spatial normalization is based on an extension and adaptation of the general method described by Shen et al (26). In that approach, a geometric model of an anatomic structure (eg, the lower spine) is first constructed from a manually labeled volumetric image. This geometric model is then trained on a number of sample images, a procedure that determines the statistical range of shape variation of this structure across individuals. This training set includes images, which are labeled by an experienced rater, obtained in randomly selected healthy individuals.

The resulting model has both geometric and statistical information about the structure of interest. It is subsequently used to automatically or semiautomatically segment and reconstruct the shape of this structure from MR images ob-

tained in an individual through a hierarchical deformation process. In this deformation process, the model deforms to adapt to edges obtained from the individual's images. At the end of this procedure, the model has adapted entirely to the individual's morphology; inverting this deformation maps the individual's images onto the template. When this procedure is applied to image data from different individuals, it brings these images into registration with the template and, therefore, with each other. We refer to our model as an adaptive focus deformable model (AFDM).

Model Construction

The concept of the stereotaxic space is largely independent from the template used in the spatial normalization procedure (10), as long as the transformation used for spatial normalization removes interindividual variability across subjects. This is analogous to the fact that the choice of a particular measurement unit, for example, the inch or the centimeter, does not affect interindividual comparisons. In practice, it is wise to choose a typical individual's spine as the template. A typical T1-weighted volumetric (set of sections) MR image was



Figure 2. Three-dimensional (3D) surface rendering of the surface model of the vertebral bodies and the spinal canal; it is composed of 837 vertices. This model was constructed from T1-weighted MR images of a typical normal spine and was subsequently trained on 13 image volumes from healthy volunteers. The resulting model combines geometric information and statistical information of the range of morphologic variation in the spine. Spatial normalization is achieved through a 3D elastic warping of patient images to the coordinate space in which this model resides.

selected by one of the authors (C.D.) to be used as the template. On the original image, we manually segmented the vertebral bodies at level L1 through S1 and the spinal canal. These structures were used as features to guide the deformation of patient MR images to the template. From the hand-labeled images, we built surface models by using the isosurface routines in mathematical software (MatLab; MathWorks, Natick, Mass). Figure 2 shows a 3D surface rendering of the surface model used in this study, and it is composed of 837 vertices.

Deformable surface models have been used extensively in the medical image analysis literature (11,21,26) for model-driven segmentation of biological structures. A deformable surface model, such as the one in Figure 2, is placed in a

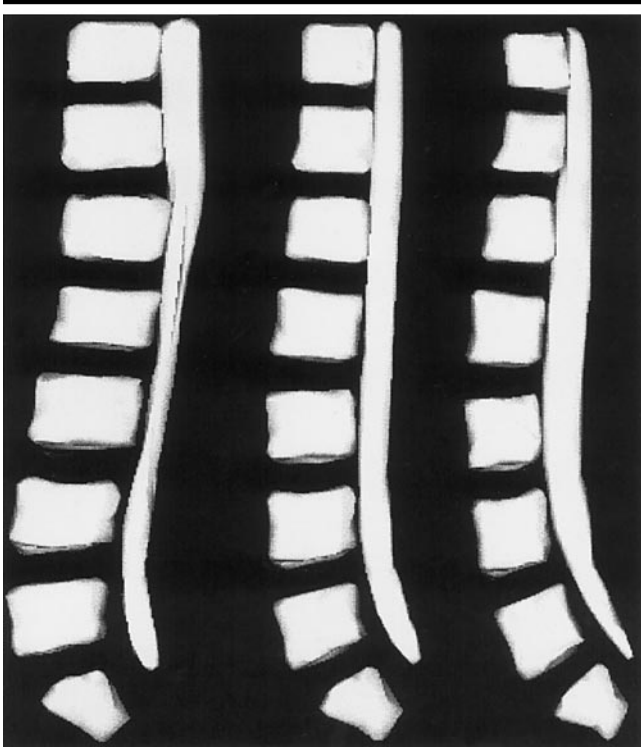


Figure 3. Three-dimensional surface rendering shows normal range of shape variation of our spine model that was quantified by the principal eigenvectors of a shape covariance matrix obtained from a number of hand-labeled spine images. The average shape of the spine in 14 subjects is shown here, within 2 SDs multiplied by the first eigenmode. The principal eigenvector (eigenmode) is the direction that explains most of the interindividual morphologic variability.

patient's volumetric image, and it subsequently deforms and attempts to conform to edges derived from the images. Since the spine model is a 3D surface model, the deformation is 3D, as well. At the end of this deformation process, the model has fully conformed to the shape of the patient's individual morphology and, thus, provides a segmentation of the individual's images in a fully or highly automated way. One of the limitations of such models has been their tendency to deform to any nearby edges in a way that can be anatomically unrealistic. For example, part of the boundary of the spinal canal can be attracted by nearby edges belonging to a vertebral body.

To remedy this situation, in the method presented herein, the concept of an attribute vector is used. An attribute vector is a set of geometric attributes associated with each vertex of our model. The attribute vector uniquely characterizes each part of the structure by quantifying its geometric properties from a local and relatively fine-grained scale to a relatively coarse scale. In this scale, global characteristics of the structure are cap-

tured. These attribute vectors uniquely characterize the different parts of the anatomy. Therefore, as the deformable surface model adapts to a patient's morphology, it seeks parts on the patient's images that have similar attribute vectors and, therefore, similar morphology.

Statistical Training of the Model

Automated segmentation of medical images with computer algorithms is a very difficult task because of the complexity of anatomic structures. Prior knowledge of the statistical shape properties of a structure of interest can greatly assist an image analysis algorithm to robustly find the structure in a patient's image, just as training improves a human rater's performance. Prior statistical knowledge is incorporated into our deformable model through a training procedure in which a small number of randomly selected images are hand labeled by an expert. The model then deforms into conformation with the hand-labeled images, thus determining a shape representation of the vertebral bodies and the spinal canal in images of each training

sample at the L1 through S1 level. This deformation is guided by the attribute vectors, which were described previously. Since each vertex on the model has a unique attribute vector, the deformation process tends to conform to the boundary of the hand-labeled images, while at the same time it seeks regions with similar attribute vectors.

The result of this procedure is a surface representation of each of the training samples, with exactly the same number of vertices, since each of the resulting surfaces is a deformed version of the model having the shape of the individual. Therefore, the statistical variation of each of the vertices can be calculated from these samples. Since the positions of these vertices are highly correlated with each other (eg, neighboring vertices undergo similar displacements), we calculated the covariance matrix of the entire collection of vertices (27,28) rather than a small covariance matrix for each vertex separately. Since the resulting covariance matrix was very large ($2,511 \times 2,511$), we determined its principal components with a standard principal component analysis and maintained only the first five of these components, which in our training data explained 98% of the total variance. These were the principal modes of shape variation (27,28), and they characterized the range of anatomic variability of the spine model. Figure 3 shows the average, within 2 SDs multiplied by the first eigenmode, of the statistical shape model.

Spatial Normalization with 3D Elastic Warping

Although spatial normalization is achieved by finding a high-dimensional spatial transformation that maps an individual's volumetric image to the template, in practice this transformation is found by warping the template to the individual's image and inverting the transformation. This warping is based on the vertebral bodies and spinal canal, which constitute the model. In particular, the deformable model of Figure 1 is superimposed on an individual's image data and subsequently deforms by maximizing conformity to edges extracted from the image. Edges are extracted by using the Canny edge detector (29), applied hierarchically at different scales, so that major edges are determined first and finer details are captured later. This deformation is controlled by the statistical and geometric information embedded in the model.

Specifically, the model does not deform arbitrarily to any nearby edge, which might lead to unrealistic deformations. Instead, it deforms by maximizing an optimization criterion and, thus, reflects a trade-off between three trends of the model. First, the model deforms to seek edges in the individual image; by conforming to an individual's spine morphology, the deformed model reflects the shape characteristics of that individual. Second, the deformed model at any instance must look like a spine or, more precisely, must lie within the range of anatomic variation embedded in the model, as represented by the principal shape components described in the previous subsection. Finally, the model deforms into configurations having similar attribute vectors, since attribute vectors reflect geometric characteristics. An example of the 3D model before and after warping to an individual spine is shown in Figure 4.

When a 3D spatial transformation from the model to the individual has been determined, then it can be inverted readily to provide a map from the individual to the template and, therefore, to the stereotaxic space in which the template resides. Since the model includes only the vertebral bodies and the spinal canal, the inverse transformation is known exactly only for those structures. Therefore, the mapping is interpolated everywhere else through 3D elastic warping. We note that elastic warping does not reflect the biomechanical properties of the spine. In fact, there is no underlying mechanical deformation taking place in spatial normalization, as, for example, in biomechanical models of the spine that are used to study instability. In our application, elastic warping is simply an interpolation scheme with several desirable properties, including its inherent smoothness and its tendency to preserve the relative locations of structures. Moreover, elastic warping has greater flexibility than several other interpolation methods, thereby accommodating the high interindividual variability in spine morphology. An example of elastic warping is shown in Figure 5.

Experiments

To generate the model, the authors collected 14 standard T1-weighted spine MR images that were obtained in 14 healthy volunteers (13 men, 1 woman), aged 25–37 years old, with a 1.5-T imaging unit (Signa; GE Medical Systems, Milwaukee, Wis) (repetition time msec/echo

time msec, 450/minimum; voxel dimensions, $0.9375 \times 0.9375 \times 3 \text{ mm}^3$, no gap). We selected the T1 contrast in part because it is commonly used and it gives an overall reasonable tissue contrast. However, other protocols can be used provided that they have sufficient contrast. Because the method depends on edges detected as described earlier, it is highly independent from the actual image intensity. Informed consent was provided by all volunteers. All identifiers were removed from the images, in accordance with our institution's institutional review board guidelines. One of the 14 volumetric images was used to generate the initial 3D model.

In this model, the vertebral bodies and spinal canal were hand labeled by one author (D.L.) by using the triplanar view of the display software distributed freely by the Brain Imaging Centre of the Montreal Neurological Institute. The isosurface routine (Mathsoft; MathWorks) of the mathematical software was subsequently used to generate a surface model from this hand-labeled image. This surface model was then deformed with the AFDM algorithm, which was previously described, into conformation with the hand-labeled images. This procedure was adaptive, with the spinal canal driving the deformation of the model initially and the more anatomically complex vertebral bodies following. It has been previously shown that this hierarchical scheme for deformation renders AFDM robust to spurious or confusing edges on the image (26).

To qualitatively demonstrate the accuracy with which the proposed method can spatially normalize volumetric images into registration with each other, we warped the remaining 13 images into the model's space and subsequently formed an average of the spatially normalized images. Statistical averages formed this way have been used extensively in the brain mapping community to represent residual interindividual anatomic variability, as was elaborated in the introduction in this article.

To qualitatively demonstrate the accuracy with which the proposed method maps patient lesions to the model's stereotaxic space for subsequent statistical analysis, we (C.D., D.L.) placed a small spherical hypothetical lesion in the L4-L5 disk for each of the 14 subjects. We then applied our method for spatial normalization, and we elastically warped all the lesions in the stereotaxic space of the template and evaluated whether the lesions were mapped to the same location.

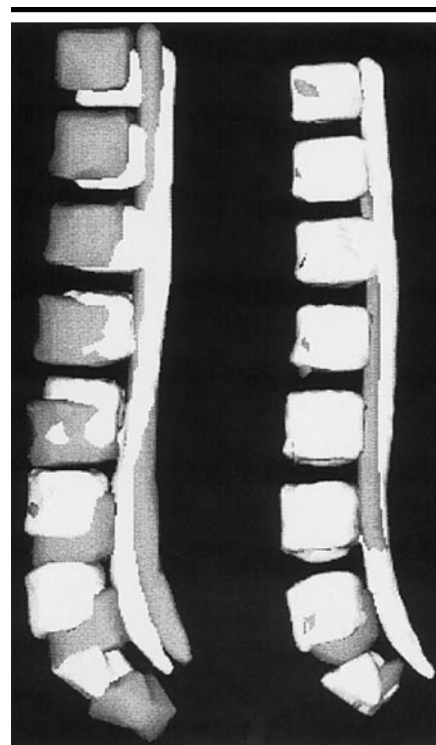


Figure 4. Three-dimensional surface rendering of the spine. Left: overlay of the model (gray) with an individual image (white) immediately after initialization of the algorithm. Right: overlay after warping of the model to the individual image. The overlay on the right shows virtually no discrepancy between gray and white and therefore shows a good registration of the warped model and the subject's spine.

Quantitation of Accuracy

Finally, to quantify the accuracy of the model-warping method, we compared manual segmentations of the vertebral bodies and the spinal canal with segmentations obtained by using the algorithm. Manual labeling was performed by one author (D.L.) and adjudicated by another (C.D.). To eliminate the bias that would otherwise be introduced if we tested our methods on the same images used to construct the statistical model, we used the leave-one-out method. In particular, recall that we trained the model on the remaining 13 images to obtain a measure of the range of statistical variation of spine morphology. We repeated this training 13 times, each time leaving one of these 13 subjects out and recalculating the statistics of shape variation from the remaining 12 images.

We then applied the resulting model to the left-out image, thus transferring the vertebral body and spinal canal labels of the template to that image. We finally

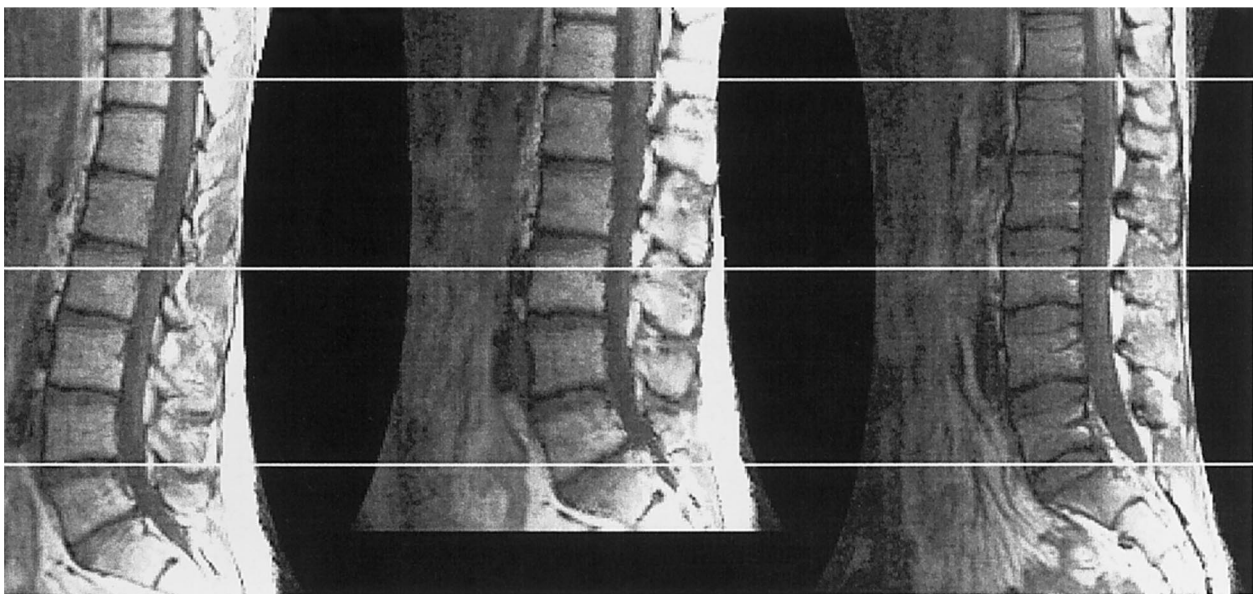


Figure 5. Comparative images of the spine. Three horizontal lines are drawn as a reference for comparisons of different levels of the spine. Left: representative section of a volumetric MR image of an individual's spine. Right: a similar section from the template. Middle: image of a spine warped to the template.

measured the volumes calculated with the algorithm versus the volumes defined manually. Manual segmentation for each subject was available, as described previously in the section regarding statistical training of the model. We determined the correlation coefficient between manual measurements and automated measurements. We also determined the average and SD of the degree of volume overlap between manual and automatic segmentation, which is a second type of error measurement.

Results

Two representative examples of the deformed model, overlaid on the corresponding subjects' images, are shown in Figure 6. To better interpret the quantitative error measurements described in the previous section and presented later, in Figure 6 we also give the respective numbers. For all subjects, the resulting average overlap between the algorithm-defined and manually defined regions was 81.5%, with an SD of 3.6%. The overlap error is accounted for by the fact that even a small disagreement, such as pixelation effects, between complex shapes typically yields a small overlap. The correlation coefficient between automatic and manual volume measurements was 0.98. The average difference between volumes of vertebral bodies and spinal canal estimated manually and with the algo-

rithm was 11.7%. We note that manual segmentation is well known to be subject to errors and interrater disagreements, as well. Because we did not have segmentations of an independent second rater, we could not compare the algorithm-rater difference with interrater differences.

We next present results from forming averages from the 14 spatially normalized images. We note that, if the spatial normalization method is perfect and achieves 100% overlap of the elastically warped images, then the average of these images will be very sharp and will have the exact morphology of the template spine. However, if significant residual variability exists after spatial normalization, it will be reflected by a fuzziness in the resulting statistical average. Figure 7 shows the average of the 14 images in our experiments, and it demonstrates high anatomic definition around the spinal canal and the vertebral bodies and, thus, reflects accurate registration of the 14 image volumes.

Finally, the average of the simulated lesions is shown in Figure 8, overlaid on the average T1-weighted MR image after warping, and indicates a very tight spatial distribution of the lesions after spatial normalization. Tightness of this spatial distribution is critical in statistical parametric mapping methods that are used to seek associations between lesion location and clinical symptoms, since those methods assume a perfect overlap

of lesions that are in anatomically corresponding regions. We note that the tightness of the spatial distribution of these lesions was achieved in the presence of a seemingly significant registration error, as indicated by the average overlap of 81.5% that was reported previously in this article. This is caused by the complexity of the anatomy of the spine, which results in large overlap errors even for small misalignment of images across subjects. This is demonstrated in Figure 9, in which two representative results are shown together with their respective overlap errors.

Discussion

We presented a new method for mapping volumetric MR image data of the spine to a stereotaxic space. We believe that this mapping, often called spatial normalization, is a key step that reduces interindividual morphologic variability, which reduces the statistical power of analyses of associations among lesion locations and clinical symptoms. The goal of spatial normalization is to place each spine lesion in the appropriate location within a canonical coordinate system and, thereby, to enable the correlation of lesion spatial and signal intensity characteristics with clinical variables.

When interindividual morphologic variability has been removed with spatial normalization, local statistical analysis can be

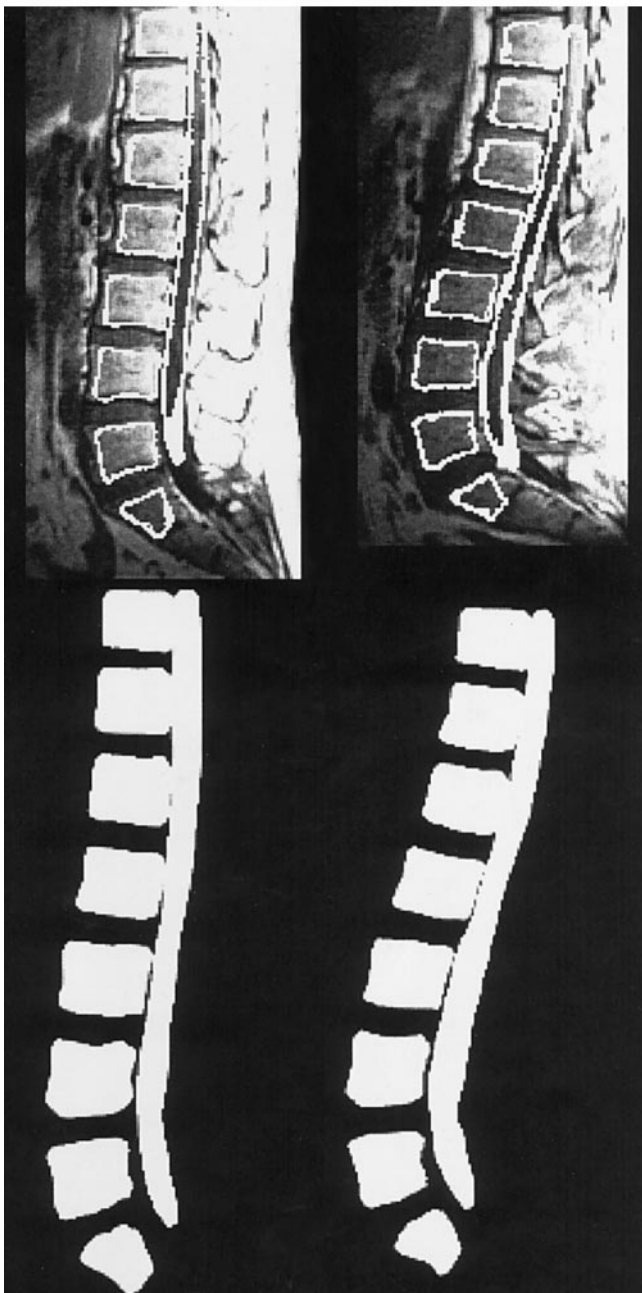


Figure 6. Images show two representative examples of the deformation of the model in Figure 1. At top, images of the spine in two different subjects are shown with the outline of the warped model overlaid. At bottom, 3D renderings of the warped configurations of the surface model are shown. The overlap between the manually defined segmentations and the corresponding algorithm-determined segmentations was 85% (for images at left) and 82% (for images at right).

performed. In the simplest case, a voxel-wise map of P values of the correlation coefficient can be calculated between a variable denoting the presence or absence of a lesion at each voxel and a measure of clinical symptoms. More elaborate statistical analyses may involve multivariate statistical models or the construction of

Bayesian models that represent complex associations between lesion locations and pain syndromes, predisposing factors, or outcome measures. In this paper, we limited our focus to spatial normalization and did not describe subsequent statistical analysis.

Extensions of our basic approach are

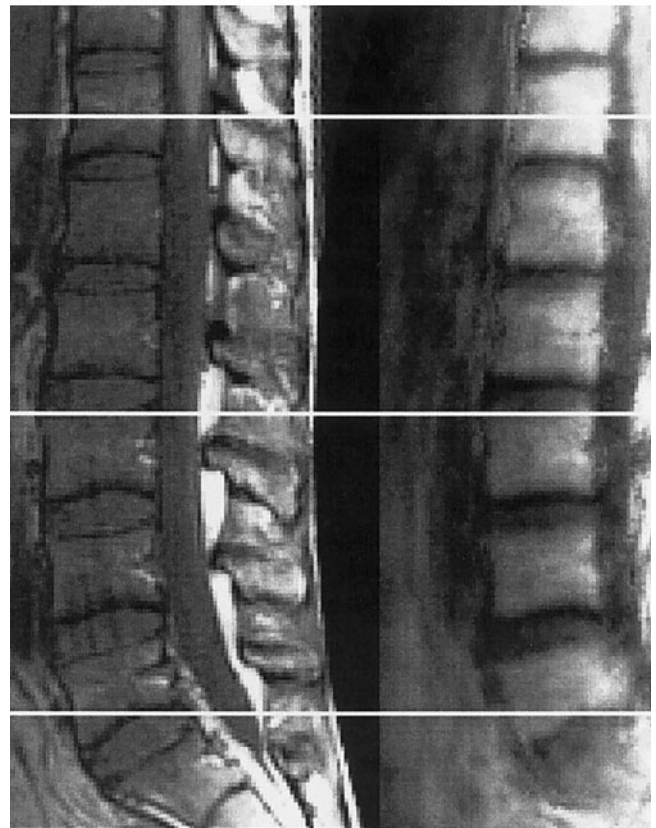


Figure 7. Images show representative section from the template's volumetric image (left) and the same section from the average image (right) formed after 13 images were elastically warped into registration with the template. The sharpness of the average image on the right is indicative of the very small residual morphologic variability in the stereotaxic space, which enables accurate and highly localized analysis between morphology and clinical symptoms, such as correlation between lesion and pain. The three horizontal lines are placed at three different transaxial levels so that the reader can compare the three images and evaluate registration accuracy.

possible, primarily in three directions. First, in this study we relied on images that had highly anisotropic voxels (ratio of 2.2 between in-plane and out-of-plane resolutions), since such images are used routinely. This amplifies partial-volume effects, particularly along lateral boundaries, which are oriented perpendicularly to the longest voxel dimension. We believe that this is the major source of error in the algorithm's performance. Isotropic image acquisition would require longer imaging time, and it might currently be considered unnecessary by radiologists. However, as the clinical utility of our method becomes established, its utility might counterbalance the additional imaging time.

Second, currently our volumetric image-warping procedure is driven by boundaries of the vertebral bodies and the spinal canal, which are the surfaces included in

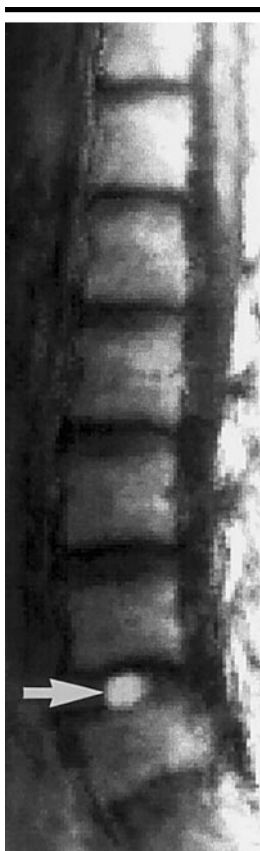


Figure 8. Spatial distribution of the average of 14 lesions after spatial normalization with the template. The lesions were originally placed within the L4-L5 disk of each subject's images and were subsequently spatially normalized according to the elastic warping transformation determined by the computer algorithm. The average spatially normalized MR image is shown in the background for reference. Tightness of this spatial distribution (arrow) is critical in statistical methods that are used to seek associations between lesion location and clinical symptoms, since those methods assume a perfect overlap of lesions that are in anatomically corresponding regions.

the model of Figure 2. As a consequence, posterior elements are bound to be registered less accurately. Extension of the model in this direction will increase the accuracy of the spatial normalization for neural foramina and facet joints, which are implicated in spinal pain syndromes.

Third, our work needs to be further applied and validated with patient data with clinically important lesions, which might reduce accuracy. However, we believe that the algorithm is particularly robust to lesions, because of the statistics embedded in it and because of its adaptive formulation, which applies higher weighting to features that are identified as normal. If a lesion is present on the image, it is likely to be properly placed in

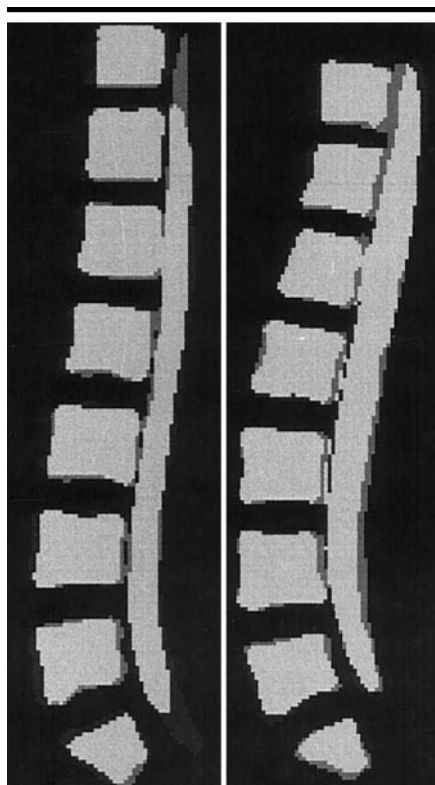


Figure 9. Three-dimensional renderings show results from automated segmentation in two representative cases. Gray corresponds to manual labeling and white shows automated segmentation. The overlap error is also reported to assist in the interpretation of the quantitative error measurements. Image at left shows an overlap percentage of 81%, and image at right shows an overlap percentage of 85%.

the stereotaxic space, on the basis of the transformation determined primarily from the normal aspects of the anatomy.

Fourth, our current approach accounts for only the gross morphology of the spine. However, as the accuracy of the shape transformation that warps a patient's image to the template increases, subtle morphologic characteristics of the spine will be captured by this shape transformation. In our previous work on the corpus callosum of the brain (10), we showed that morphologic analyses that are based on the properties of this shape transformation can reveal localized and subtle effects. For example, an unusual focal stretching of a patient's images when they are being matched to a normal individual's spine images may reflect an underlying stenosis of the central canal for that patient. Similarly, abnormal bone growth, such as osteophyte formation, can be detected as an abnormal contraction of the shape transformation that maps a patient's images to the template.

Work with these concepts is under way in our laboratory.

APPENDIX

Clinical measurements, such as laboratory values, and physical examination and history assessments, must be comparable across physicians and medical centers if they are to be meaningful in the contexts of patient care and research. Similarly, a key issue in stereotaxic analysis methods is spatial normalization, a procedure that warps an individual's image data into registration with an anatomic template and, thus, makes these image data comparable across individuals. This anatomic template can be a typical subject's volumetric image, or it can be a product of some form of statistical shape averaging. This step is important, since it places anatomically corresponding regions in the same location in the stereotaxic space (Fig 1).

We use the term *lesion* in this article to indicate any signal intensity or morphologic abnormality in image data. Suppose that a lesion (shown as a circle in Fig 1) at a particular level of the spine always causes a particular pain syndrome. Assume that a large number of patient images are used in a data-mining paradigm in which an attempt is made to identify such lesion-pain relationships. In that paradigm, one would ask the following question: Is the presence of a lesion at a location with coordinates x , y , and z correlated with the presence of the pain syndrome?

In general, if the data are placed in the reference system of the database without spatial normalization, as in Figure 1, A, then the answer to the statistical query just mentioned may be negative, due to loss of statistical power. Ideally, one would like to position the patient images in the coordinate system of the database, as shown in Figure 1, B, where corresponding spine levels have the same coordinates (ie, x , y , z). In a more realistic scenario, Figure 1, C, may be sufficient to allow detection of this lesion-pain association, provided that the lesions have enough spatial overlap. The goal of spatial normalization is to properly position the data in the stereotaxic space by eliminating or reducing interindividual morphologic variability.

Acknowledgments: The authors thank David M. Yousem, MD, and Don M. Long, MD, PhD, for their support of this project.

References

1. Long DM, BenDebba M, Torgeson WS. Persistent back pain and sciatica in the United States: patient characteristics. *J Spinal Dis* 1996; 9:40-58.
2. Deyo RA, Cherkin D, Conrad D, Volin E. Cost, controversy, crisis: low-back pain

- and the health of the public. *Ann Rev Pub Health* 1991; 12:141–156.
3. Scientific approach to the assessment and management of activity-related spinal disorders: a monograph for clinicians—report of the Quebec Task Force on Spinal Disorders. *Spine* 1987; 12 (7 suppl):S1–S59.
 4. Talairach J, Tournoux P. Co-planar stereotaxic atlas of the human brain. Stuttgart, Germany: Thieme, 1988.
 5. Fox PT, Mintum MA, Reiman EM, Reichle ME. Enhanced detection of focal brain responses using inter-subject averaging and distribution analysis of subtracted PET images. *J Cereb Blood Flow Metab* 1988; 8:642–653.
 6. Evans AC, Beil C, Marrett S, Thompson CJ, Hakim A. Anatomical-function correlation using an adjustable MRI-based region of interest atlas with positron emission tomography. *J Cereb Blood Flow Metab* 1988; 8:513–530.
 7. Friston KJ, Holmes AP, Worsley KJ, Poline JP, Frith CD, Frackowiak RS. Statistical parametric maps in functional imaging: a general linear approach. *Hum Brain Mapp* 1995; 2:189–210.
 8. Letovsky SI, Whitehead SH, Paik CH, et al. A brain image database for structure/function analysis. *AJNR Am J Neuroradiol* 1998; 19:1869–1877.
 9. Herskovits EH, Megalooikonomou V, Davatzikos C, Chen A, Bryan RN, Gerring JP. Is the spatial distribution of brain lesions associated with closed-head injury predictive of subsequent development of attention-deficit hyperactivity disorder? Analysis with a brain-image database. *Radiology* 1999; 213:389–394.
 10. Davatzikos C, Vaillant M, Resnick S, Prince JL, Letovsky S, Bryan RN. A computerized approach for morphological analysis of the corpus callosum. *J Comput Assist Tomogr* 1996; 20:88–97.
 11. Davatzikos C. Mapping of image data to stereotaxic spaces: applications to brain mapping. *Hum Brain Mapp* 1998; 6:334–338.
 12. Thompson PM, MacDonald D, Mega MS, Holmes CJ, Evans AC, Toga AW. Detection and mapping of abnormal brain structure with a probabilistic atlas of cortical surfaces. *J Comput Assist Tomogr* 1997; 21:567–581.
 13. Miller MI, Christensen GE, Amit Y, Grenander U. Mathematical textbook of deformable neuroanatomies. *Proc Natl Acad Sci U S A* 1993; 90:11944–11948.
 14. Ashburner J, Friston KJ. Voxel-based morphometry: the methods. *Neuroimage* 2000; 11:805–821.
 15. Ashburner J, Hutton C, Frackowiak R, Johnsrude I, Price C, Friston K. Identifying global anatomical differences: deformation-based morphometry. *Hum Brain Mapp* 1998; 6:348–357.
 16. Woermann FG, Free SL, Koeppe MJ, Ashburner J, Duncan JS. Voxel-based comparison of automatically segmented cerebral gray matter: a rater-independent comparison of structural MRI in patients with epilepsy. *Neuroimage* 1999; 10:373–384.
 17. Gaser C, Voltz HP, Kiebel S, Riehemann S, Sauer H. Detecting structural changes in whole brain based on nonlinear deformations: application to schizophrenia research. *Neuroimage* 1999; 10:107–113.
 18. Freeborough PA, Fox NC. Modeling brain deformations in Alzheimer's disease by fluid registration of serial MR images. *J Comput Assist Tomogr* 1998; 22:838–843.
 19. Machado AM, Gee JC, Campos MF. A factor analytic approach to structural characterization. Proceedings of the IEEE Workshop on Mathematical Methods in Biomedical Image Analysis, IEEE Computer Society, 2000; 219–226.
 20. Davatzikos C. Spatial normalization of 3D images using deformable models. *J Comput Assist Tomogr* 1996; 20:656–665.
 21. Thompson PM, Schwartz C, Toga AW. High resolution random mesh algorithms for creating a probabilistic 3D surface atlas of the human brain. *Neuroimage* 1996; 3:19–34.
 22. Collins DL, Neelin P, Peters TM, Evans AC. Automatic 3D intersubject registration of MR volumetric data in standardized Talairach space. *J Comput Assist Tomogr* 1994; 18:192–205.
 23. Christensen GE, Rabbitt RD, Miller MI. Deformable templates using large deformation kinematics. *IEEE Trans Med Imaging* 1996; 5:1435–1447.
 24. Bookstein FL. Principal warps: thin-plate splines and the decomposition of deformations. *IEEE Trans Pattern Anal Machine Intell* 1989; 11:567–585.
 25. Kochunov PV, Lancaster JL, Fox PT. Accurate high-speed spatial normalization using an octree method. *Neuroimage* 1999; 10:724–737.
 26. Shen D, Herskovits EH, Davatzikos C. An adaptive-focus statistical shape model for segmentation and shape modeling of 3-D brain structures. *IEEE Trans Med Imaging* 2001; 20:257–270.
 27. Cootes FT, Taylor CJ. Combining point distribution models with shape models based on finite element analysis. *Image Vis Comput* 1995; 13:403–409.
 28. Shen D, Moffat S, Resnick SM, Davatzikos C. Measuring size and shape of the hippocampus in MR images using a deformable shape model. *Neuroimage* 2002; 15:422–434.
 29. Canny J. A computational approach to edge detection. *IEEE Trans Pattern Anal Mach Intell* 1996; 8:679–698.